Image potential and the exchange-correlation weighted density approximation functional

P. García-González,[1,2] J. E. Alvarellos,[1] E. Chacón,[3] and P. Tarazona[4]
[1]*Departamento de Física Fundamental, Universidad Nacional de Educación a Distancia, Apartado 60.141, E-28080 Madrid, Spain*
[2]*Department of Physics, University of York, Heslington, York YO10 5DD, United Kingdom*
[3]*Instituto de Ciencias de Materiales, Consejo Superior de Investigaciones Científicas, Cantoblanco, E-28049 Madrid, Spain*
[4]*Departamento de Física Teórica de la Materia Condensada and Instituto Nicolás Cabrera, Universidad Autónoma de Madrid, E-28049 Madrid, Spain*
(Received 20 June 2000)

It is known that the exchange-correlation (XC) potential v_{XC} obtained by using the weighted density approximation (WDA) does not yield the correct image behavior $-1/4z$ outside a metal surface. Some authors have speculated that this limitation could be overcome by symmetrizing the XC hole, using a two-point scaling factor in its modelization by the WDA. In this work, we show that this symmetrization procedure does not improve the XC potential v_{XC}, and makes it unphysical. Alternatively, we present a WDA scheme based on an anisotropic scaling for the XC hole, constructed to verify both the normalization of the XC hole *and* the exact value of the second momenta of the XC hole. In this last case, the potencial v_{XC} has the correct image decay.

I. INTRODUCTION

Density-functional theory (DFT) (Ref. 1) has been widely used in the study of structural and electronic properties of solids, molecules, and atoms. However, most of the functional schemes fail to reproduce the correct asymptotic behavior of the exchange-correlation (XC) potential v_{XC} and, in particular, its imagelike decay $-\frac{1}{4}z$ far outside a metal surface (z is the coordinate normal to the surface). Although the image potential has very little influence on such properties as density profiles, work functions, and surface energies, it is crucial to describe the existence of image states and when determining the vacuum gap in scanning tunneling microscopy.[2,3]

As it is very well known, the local-density approximation (LDA) gives an exponentially decaying v_{XC} outside a metal surface.[4] On the other hand, the generalized-gradient approximation, which is the current standard in DFT calculations, does not provide the correct image behavior either.[5] These results are not a surprise, since the potential decay of v_{XC} is an outcome of the highly nonlocal nature of the XC energy functional $E_{\mathrm{XC}}[n]$. Therefore, it is very unlikely that simple semilocal approaches will provide the correct image potential. On the other hand, the XC potential is given by the functional derivative $v_{\mathrm{XC}}(\mathbf{r})=\delta E_{\mathrm{XC}}[n]/\delta n(\mathbf{r})$ and, as a consequence, the image behavior obtained by means of interpolation procedures focused on v_{XC}, as the one developed by Serena *et al.*[6] lacks functional consistency because the interpolated v_{XC} is not the first functional derivative of any functional $E_{\mathrm{XC}}[n]$.

A similar limitation reads for the v_{XC} potential arising from the Sham-Schlüter equation[7] within the framework of the GW approximation.[8] Using this scheme, Eguiluz and coworkers obtained the XC potential for a jellium surface showing the correct asymptotic behavior.[9,10,3] The main decay ($\sim -\frac{1}{4}z$) is due to the Coulomb interaction, whereas the exchange potential is found to decay faster ($\propto z^{-2}$). The latter result was also obtained by Solomatin and Sahni[11] by analyzing the exact exchange potential given by the optimized potential method.[12] The same trends are also shown by the dynamic XC potential of a realistic Al(111) surface.[13] Note that by using the GW approximation, it is also possible to obtain the total energy of the electron system. However, the overall accuracy of this many-body approach to calculate ground-state properties is still unclear.[14,15]

The goal of this work is to provide clues in the development of an XC energy functional able to give not only the energy of an electron system but also the imagelike behavior of v_{XC} in a metal surface. With this aim in mind, the nonlocal weighted density approximation (WDA) (Ref. 16) could be considered as a good approach to the problem that concerns us, because the WDA improves almost systematically the results obtained with the local and semilocal functionals for a wide variety of problems.[17] The starting point of the WDA is the exact expression for the XC energy (atomic units are used throughout this paper),

$$E_{\mathrm{XC}}[n]=\tfrac{1}{2}\int d\mathbf{r}\, n(\mathbf{r})\int d\mathbf{r}'\frac{n_{\mathrm{XC}}(\mathbf{r},\mathbf{r}')}{|\mathbf{r}-\mathbf{r}'|}, \tag{1}$$

where $n_{\mathrm{XC}}(\mathbf{r},\mathbf{r}')$ is the XC hole centered at $\mathbf{r}$, which is defined as

$$n_{\mathrm{XC}}(\mathbf{r},\mathbf{r}')=n(\mathbf{r}')\int_0^1 d\gamma\, g_\gamma(\mathbf{r},\mathbf{r}')=n(\mathbf{r}')G(\mathbf{r},\mathbf{r}'). \tag{2}$$

$g_\gamma(\mathbf{r},\mathbf{r}')$ is the pair-correlation function (PCF) of an electron system whose ground-state density is $n(\mathbf{r})$, but with an interaction potential γ/r. In the WDA, the unknown XC hole (2) is approximated by replacing, at each point $\mathbf{r}$, the integrated PCF $G(\mathbf{r},\mathbf{r}')$ by the $G_{\mathrm{hom}}(n,r)$ corresponding to a homogeneous electron gas but evaluated at a different $\tilde{n}(\mathbf{r})$:

$$n_{\mathrm{XC}}^{\mathrm{WDA}}(\mathbf{r},\mathbf{r}')=n(\mathbf{r}')G_{\mathrm{hom}}(\tilde{n}(\mathbf{r}),|\mathbf{r}-\mathbf{r}'|). \tag{3}$$

The *weighted density* $\tilde{n}(\mathbf{r})$ is determined by imposing the exact sum rule for the XC hole,

$$\int d\mathbf{r}\, n_{\mathrm{XC}}(\mathbf{r},\mathbf{r}') = -1. \tag{4}$$

However, since $G_{\mathrm{hom}}(n,r)$ is unknown, we need to approximate this function as well. This is done by using parametrized forms, developed in such a way that the energy of the homogeneous electron gas is recovered. In this work, we will use the self-consistent proposal by Chacón and Tarazona[18] (whose shape is not very different from the more sophisticated parametrization by Perdew and Wang[19]), which allows us to scale G_{hom} as

$$G_{\mathrm{hom}}(n,r) \simeq C[\zeta(k_F)]\hat{G}[2\zeta(k_F)r], \tag{5}$$

where $k_F=(3\pi^2 n)^{1/3}$, $\zeta(k_F)=k_F/\lambda(k_F)$, the dimensionless functions C and λ are determined by the XC density energy, and $\hat{G}$ is a parametrized one. Using this scaled integrated PCF (5), for an inhomogeneous system we can write

$$G^{\mathrm{WDA}}(\mathbf{r},\mathbf{r}') = C(\zeta(\mathbf{r}))\hat{G}[2\zeta(\mathbf{r})|\mathbf{r}-\mathbf{r}'|], \tag{6}$$

where the short-hand notation $\zeta(\mathbf{r})=\zeta(\tilde{k}_{\mathrm{F}}(\mathbf{r}))$, with $\tilde{k}_{\mathrm{F}}(\mathbf{r}) = [3\pi^2\tilde{n}(\mathbf{r})]^{1/3}$, has been used.

The WDA significantly improves the LDA behavior of v_{XC} far outside a metal surface, and reproduces the potential decay $\propto z^{-1}$. Unfortunately, when using any realistic short-ranged function $\hat{G}$, the numerical coefficient of the decaying tail is $-\frac{1}{2}$ instead of the exact value $-\frac{1}{4}$. The latter can be obtained using a long-ranged function $\hat{G}$ in Eq. (6),[20,21] but at the expense of getting unphysical results for the position of the image plane[6,22] and unreasonable surface energies.[23]

Several authors have considered that the incorrect value $-\frac{1}{2}$ is an intrinsic limitation of the WDA due to the use of a nonsymmetric PCF for an inhomogeneous system.[17] In the first part of this work, we present a modification of the WDA which keeps the exact relation $G(\mathbf{r},\mathbf{r}')=G(\mathbf{r}',\mathbf{r})$. To do so, we use a two-point function $\xi(\mathbf{r},\mathbf{r}')$, rather than the one-point function $\zeta(\mathbf{r})$ in Eq. (6). Using this *symmetrized* WDA (sWDA), we have studied the asymptotic behavior of the XC potential, finding that there is no improvement at all with respect to the original WDA. Actually, the symmetrization worsens the overall shape of v_{XC}. This surprising result is related to the fact that the relevant quantity in the WDA is the XC hole, not the integrated PCF: the use of a more complicated scaling in Eq. (6) only introduces minor changes in $n_{\mathrm{XC}}(\mathbf{r},\mathbf{r}')$ (and, therefore, in the XC energy) but it has undesirable consequences when calculating the functional derivative of $E_{\mathrm{XC}}[n]$.

Bearing in mind that the WDA must mainly be viewed as an approximation to $n_{\mathrm{XC}}(\mathbf{r},\mathbf{r}')$, in the second part of this paper we present another modification of the WDA, which tries to directly improve the behavior of the XC hole. As in the sWDA, we use an anisotropic scaling in the homogeneous PCF. However, instead of imposing the condition $G(\mathbf{r},\mathbf{r}')=G(\mathbf{r}',\mathbf{r})$, we obtain the value of such scaling using not only the sum rule (4) but also a sum rule related to the second momenta of the distribution $n_{\mathrm{XC}}(\mathbf{r},\mathbf{r}')$. Using this ansatz, we show that the v_{XC} so obtained exhibits the correct imagelike limit $-\frac{1}{4}z$ outside the metal, whereas the XC hole spreads laterally on the surface for high values of z.

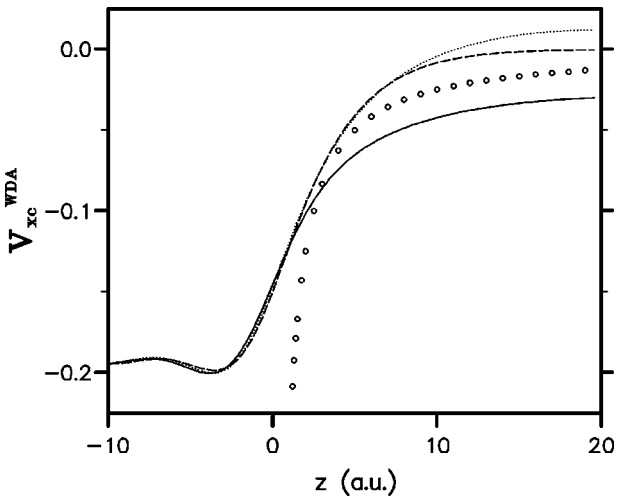

FIG. 1. The WDA (solid line), the sWDA (dotted line), and the LDA (dashed line) values for the XC potential $v_{\mathrm{XC}}(z)$, in atomic units, for a semi-infinite jellium system with $r_s=3.93a_0$. The electron density profile used is the one resulting from a LDA calculation. The circles represent the classical image potential $-\frac{1}{4}z$.

II. SYMMETRIZED WDA

As we have previously commented, our first attempt is to modify the original WDA in order to overcome the lack of symmetry of the integrated PCF $G^{\mathrm{WDA}}(\mathbf{r},\mathbf{r}')$ given in Eq. (6). The simplest way to do so is to modify Eq. (6) considering a symmetrized scaling factor $\xi(\mathbf{r},\mathbf{r}')$:

$$G^{\mathrm{sWDA}}(\mathbf{r},\mathbf{r}') \simeq C(\xi(\mathbf{r},\mathbf{r}'))\hat{G}[2\xi(\mathbf{r},\mathbf{r}')|\mathbf{r}-\mathbf{r}'|]. \tag{7}$$

Because we can only use the sum rule (4) to fit the scaling, $\xi(\mathbf{r},\mathbf{r}')$ has to be a function of the weighted density evaluated at the points $\mathbf{r}$ and $\mathbf{r}'$. Therefore, we can use a similar ansatz to that used in the symmetrized *averaged density approximation* for the kinetic-energy functional:[24]

$$\xi(\mathbf{r},\mathbf{r}') = 2^{-1/\beta}[\zeta(\mathbf{r})^{\beta}+\zeta(\mathbf{r}')^{\beta}]^{1/\beta}, \tag{8}$$

where β is a free parameter and, as in the original WDA, $\zeta(\mathbf{r})=\tilde{k}_F(\mathbf{r})/\lambda(\tilde{k}_F(\mathbf{r}))$. By varying the value of β, different (arithmetic, geometric, etc.) means of the scalings $\zeta(\mathbf{r})$ and $\zeta(\mathbf{r}')$ can be covered.

When compared with the original WDA, the evaluation of $\tilde{n}(\mathbf{r})$ [or equivalently of $\tilde{k}_F(\mathbf{r})$] is much more involved, because the sum-rule condition (4) now yields a set of coupled integral equations that must be solved iteratively. On the other hand, when calculating $v_{\mathrm{XC}}(\mathbf{r})$, a matrix equation must be solved, instead of a simple evaluation of a double integral. Nevertheless, for a jellium surface the sWDA functional can be handled with an affordable numerical effort (see the Appendix for details) due to the translational invariance of the system along the x-y plane.

In Fig. 1, we present the XC potential for a jellium surface with $r_s=4a_0$, as obtained with the original WDA and with the sWDA (with $\beta=\frac{1}{2}$). We are mainly interested in the changes induced by the symmetrization, so we have calcu-

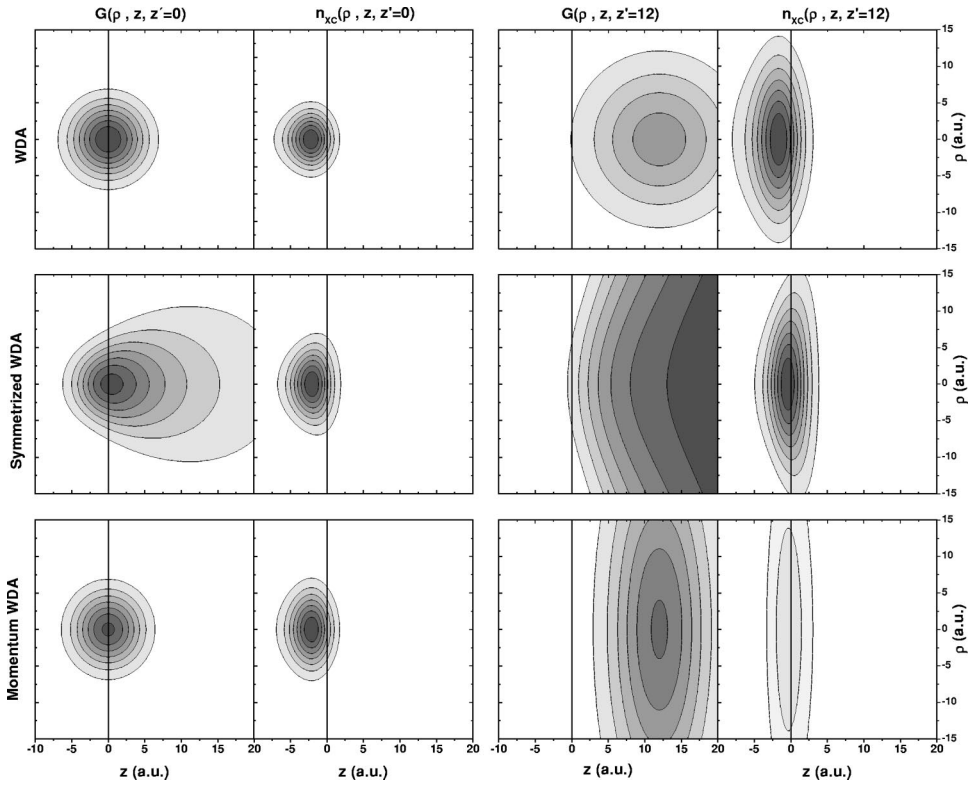

FIG. 2. Integrated pair correlation function $G(\rho,z,z')$ (the first, $z'=0$, and the third column, $z'=12a_0$) and the corresponding XC hole $n_{\mathrm{XC}}(\rho,z,z')$ (the second and fourth column) for a semi-infinite jellium system with $r_s=4a_0$. WDA: first row; sWDA: second row; mWDA: third row. Each column has the same values for the contour lines; in the darker regions, the values of the functions are higher.

lated the functional derivative of E_{XC} using the same electronic profile in both cases (specifically, in this paper we use the LDA profiles obtained with the Lang and Kohn method[4] using the XC energy density parametrized by Chacón and Tarazona[18]). As we commented on in the Introduction, the asymptotic behavior of $v_{\mathrm{XC}}^{\mathrm{WDA}}(z)$ equals $-\frac{1}{2}z$. However, $v_{\mathrm{XC}}^{\mathrm{sWDA}}(z)$ goes to an unphysical constant when $z\gg 0$. We have tried several values of β, as well as different short-ranged parametrizations for $\hat{G}$, but $v_{\mathrm{XC}}^{\mathrm{sWDA}}(z)$ always shows that behavior. Therefore, we can conclude that a straightforward symmetrization of the WDA integrated PCF is not enough to obtain the correct imagelike potential and, moreover, the results obtained with the functional are clearly worse than those obtained with the original WDA one.

In order to understand this amazing outcome, we present in Fig. 2 the integrated PCFs $G(\mathbf{r},\mathbf{r}')=G(z,z',\rho')$, being $\rho'=\sqrt{(x-x')^2+(y-y')^2}$, obtained using both functionals, and the LDA profile, for two values of z: the first one when z is at the edge of the positive background ($z=0$), and the second when z is located far outside the surface ($z=12a_0$). As can be seen, $G^{\mathrm{WDA}}(z,z',\rho')$ always has spherical symmetry around the point z, whereas for the sWDA functional (with $\beta=\frac{1}{2}$) the higher the value of z is, the more anisotropic $G^{\mathrm{sWDA}}(z,z',\rho')$ becomes. Comparing these results with recent Monte Carlo calculations,[25] it seems at first glance that the sWDA improves the description of the integrated PCF. However, we must remember that the key quantity in the WDA is the XC hole $n_{\mathrm{XC}}(\mathbf{r},\mathbf{r}')$ and, as we can also see in Fig. 2, the XC holes obtained with both models are rather similar. In fact, for $z\gg 0$, neither the function $n_{\mathrm{XC}}^{\mathrm{WDA}}(z,z',\rho')$ nor $n_{\mathrm{XC}}^{\mathrm{sWDA}}(z,z',\rho')$ show any evident lateral spread over the surface. As a conclusion, the anisotropy induced by the two-point scaling factor $\xi(z,z')$ is not enough to improve the shape of the XC hole, this shape being still monitored by the dependence on $|\mathbf{r}-\mathbf{r}'|$.

III. MOMENTUM WDA

In the preceding section, we have seen that, in order to improve the description of the XC potential in a metal surface, we need to develop a better model for the XC hole. In the WDA, the hole $n_{\mathrm{XC}}(\mathbf{r},\mathbf{r}')$ around the point $\mathbf{r}$ verifies the sum rule (4), which fixes the value of the zeroth momentum of n_{XC}. However, additional information about the shape of the hole around $\mathbf{r}$ can be obtained from the values of its normalized second momenta, given by

$$M_{ij}(\mathbf{r})=-\int d\mathbf{r}'\frac{x_i'x_j'}{|\mathbf{r}'|^2}n_{\mathrm{XC}}(\mathbf{r},\mathbf{r}+\mathbf{r}')G(\mathbf{r},\mathbf{r}+\mathbf{r}'), \qquad (9)$$

where $i,j=1,2,3$ represent the Cartesian axes. *A priori*, the tensor $M_{ij}(\mathbf{r})$ is unknown for any electron system. Nevertheless, due to the symmetry, for the homogeneous electron gas we have

$$M_{ij}=\begin{cases}1/3 & \text{if } i=j\\ 0 & \text{otherwise.}\end{cases} \qquad (10)$$

On the other hand, if we consider a jellium surface, when $z\gg 0$ the XC hole can be approximately described by the classical one (i.e., by the screening charge induced on the surface of the metal). That is,

$$n_{\mathrm{XC}}(z\gg 0,\mathbf{r}')\simeq -\frac{z\,\delta(z'-z_0)}{2\pi[(\rho')^2+z^2]^{3/2}}, \qquad (11)$$

where δ is the Dirac delta function and z_0 is the position of the image plane. It is easy to show that Eq. (11) also verifies the equality (10). Therefore, since the relation (10) for a metal surface is satisfied both in the bulk and in the vacuum, we assume that our approximated XC hole verifies Eq. (10) across the surface, i.e., $M_{jj}(z)=\frac{1}{3}$ for any value of z. In

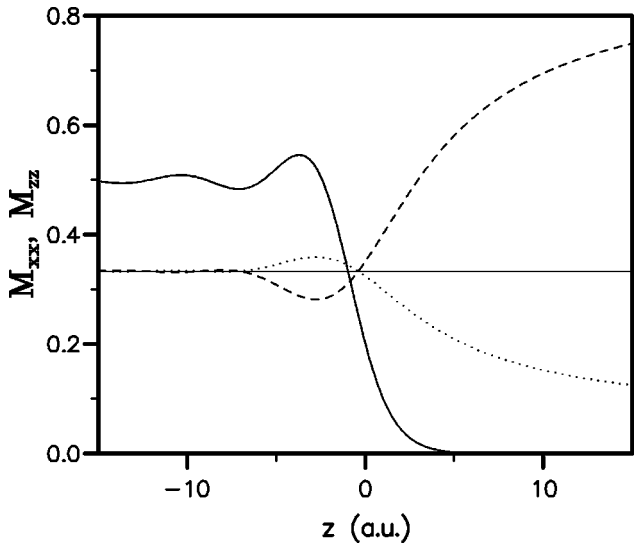

FIG. 3. The dimensionless momenta $M_{xx}(z)$ (dotted line) and $M_{zz}(z)$ (dashed line) given by the WDA for a jellium surface with $r_s=4a_0$. The full line shows, as a reference, the electronic density profile used, in arbitrary units.

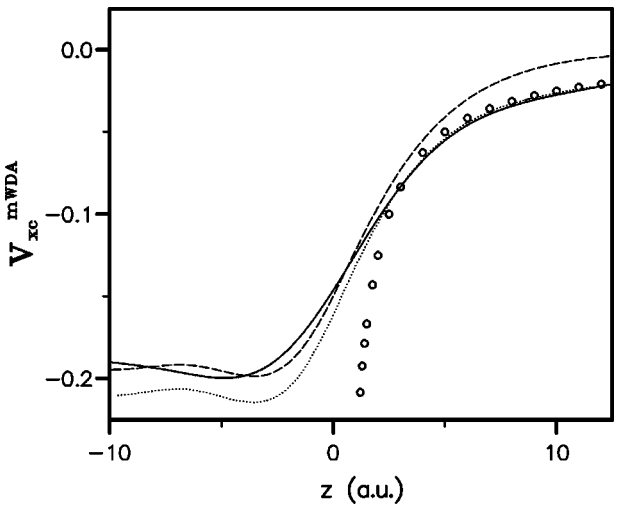

FIG. 4. The XC potential, in atomic units, given by the mWDA model (solid line) for a semi-infinite jellium system with $r_s=3.93a_0$. The dashed line shows the LDA results. The dotted line is the calculation by Eguiluz and co-workers (Ref. 10) using the GW approximation. The circles represent the classical image potential $-\frac{1}{4}z$.

order to better appreciate this approximation, we show in Fig. 3 the values for $M_{xx}(z)=M_{yy}(z)$ and $M_{zz}(z)$ obtained with the original WDA functional for the LDA profile. As expected, inside the metal both momenta take the value $\frac{1}{3}$, close to the surface these functions deviate slightly from this value, and only well outside the surface are they very different from $\frac{1}{3}$, because the WDA PCF is completely inaccurate for $z\gg 0$. So, our assumption will not force the original WDA scheme too much within the region where it gives good results; moreover, it will improve over the behavior of the WDA momenta when $z\gg 0$. In short, our approach to the XC hole for a metal surface is determined by the sum rule (4) and by the two additional conditions $M_{xx}(z)=M_{yy}(z)=\frac{1}{3}$ and $M_{zz}(z)=\frac{1}{3}$.

To fulfill these new sum rules, we have to change the WDA modeling of the integrated PCF. We propose the following ansatz (which we call mWDA):

$$G^{\mathrm{mWDA}}(\mathbf{r},\mathbf{r}')=C(\zeta(\mathbf{r}))\hat{G}[2\zeta(\mathbf{r})\|\mathcal{H}(\mathbf{r})(\mathbf{r}-\mathbf{r}')\|], \quad (12)$$

where $\mathcal{H}(\mathbf{r})$ is a *deformation* matrix to be obtained by imposing the aforementioned sum rules for the second momenta. Note that if we set $\mathcal{H}(\mathbf{r})=1$, we recover the original WDA model, whereas $\mathcal{H}(\mathbf{r})\neq 1$ breaks the spherical symmetry of the integrated PCF. Due to the symmetry of the jellium surface, the matrix $\mathcal{H}$ is diagonal and $\mathcal{H}_{xx}(\mathbf{r})=\mathcal{H}_{yy}(\mathbf{r})$. Therefore,

$$G^{\mathrm{mWDA}}(\mathbf{r},\mathbf{r}')$$
$$=C(\zeta(z))\times\hat{G}[2\zeta(z)\sqrt{\mathcal{H}_{xx}^2(z)(\rho')^2+\mathcal{H}_{zz}^2(z)(z-z')^2}],$$

and, for each point z, we have three sum rules which allow us to obtain $\tilde{n}(z)$ [or $\zeta(z)$], $\mathcal{H}_{xx}^2(z)$, and $\mathcal{H}_{zz}^2(z)$. The integrated PCF obtained for the LDA profile is plotted in Fig. 2. As for the G^{sWDA}, the deformation of G^{mWDA} has an overall agreement with the Monte Carlo results[25] in the regions outside the surface. On the other hand, the spurious spread inside the vacuum that appeared in the sWDA has been eliminated. Finally, the XC hole obtained when $z\gg 0$ is definitely extended over the surface, featuring an evident change with respect to the WDA and sWDA results (note that each column in the figure has the same values for the contour lines).

The shape of $v_{\mathrm{XC}}(z)$ obtained with this new mWDA functional is shown in Fig. 4, when the LDA profile is used. We have to point out that the functional derivative $\delta E_{\mathrm{XC}}^{\mathrm{mWDA}}[n]/\delta n(\mathbf{r})$ has been obtained numerically, by analyzing the change induced in the XC energy by a small perturbation in the density profile at each point $\mathbf{r}$. Our calculation yields numerical errors for very high values of z ($z>15a_0$), but it is enough to demonstrate that the mWDA functional gives the correct asymptotic behavior, $-\frac{1}{4}z$. In fact, for $z<2a_0$ there are minor differences between $v_{\mathrm{XC}}^{\mathrm{WDA}}(z)$ and $v_{\mathrm{XC}}^{\mathrm{mWDA}}(z)$, but for $z>2a_0$ they have a very different behavior.

On the other hand, as shown in the same figure, $v_{\mathrm{XC}}^{\mathrm{mWDA}}(z)$ fits very well the XC potential presented by Eguiluz *et al.* using the Sham-Schlüter equation.[3] The differences between $v_{\mathrm{XC}}^{\mathrm{mWDA}}(z)$ and $v_{\mathrm{XC}}^{GW}(z)$ in the bulk region appear because different XC density energies are used in each case.

IV. CONCLUSIONS

In this work, we have studied the capability of the WDA scheme to reproduce the image-potential limit of v_{XC} in the vacuum region of a metal surface. We have presented two modifications of the WDA model, trying to overcome the incorrect behavior of the XC functional.

The first model, sWDA, uses a two-point function as the scaling factor $\xi(\mathbf{r},\mathbf{r}')$ and uses the sum-rule condition (4) to evaluate $\tilde{n}(\mathbf{r})$. The new functional has a symmetric integrated PCF, but gives an unphysical XC potential.

The second model, mWDA, breaks down the $|\mathbf{r}-\mathbf{r}'|$ dependence of $G(\mathbf{r},\mathbf{r}')$ by imposing two conditions that the XC hole has to verify: first, as in the original WDA and in the sWDA, the zeroth-order momenta of the XC hole, i.e.,

TABLE I. Surface energy (in erg/cm^2) obtained with the LDA self-consistent density profile for a jellium surface using the LDA functional and the WDA models described in the text.

r_s	LDA	WDA	sWDA $\beta=0.5$	mWDA
2	3361.1	3323.1	3533.1	3442.8
3	762.6	761.4	820.0	808.8
4	260.0	262.6	286.3	286.1
5	109.9	112.6	124.3	126.3

the sum rule (4); second, and this is a new condition for any proposed functional, at each point $\mathbf{r}$ the hole $n_{\rm XC}^{\rm mWDA}$ must satisfy the values of the second momenta of the exact XC hole. This second condition introduces an anisotropic scaling of the XC hole on the density profile. In general, the exact momenta are not known, but for a jellium system it is easy to obtain these values both in the bulk region and very outside the metal (with the same values in both limits). Assuming as an ansatz that these momenta are constant across the surface, we can obtain the deformation matrix and, therefore, evaluate the XC functional. The XC potential, i.e., the functional derivative of the energy functional so constructed, shows the correct asymptotic behavior, with results close to the original WDA ones in the surface region.

A number of questions remain open. First of all, we have to generalize the mWDA model for any system and it is not easy to anticipate the values of the momenta of the XC hole in a more general case. In this work, we have seen that good results are obtained when imposing simple momenta conditions. It might also be the case for other systems and the possibility of obtaining similar conditions for the momenta in localized systems is presently under study.

Though the aim of this paper is the discussion of the XC potential at the jellium surface, we are now presenting some preliminary results for the surface energies in Table I, as obtained with the WDA functionals described in this work. These energies are evaluated for the same LDA electronic density profile. We can see that the results given by the sWDA and by the mWDA are very similar, and are systematically bigger than the LDA and WDA energies (which are almost the same). These results, however, do not confirm the trend showed by those obtained using wave-function-based methods as the Fermi hypernetted chain[26] or the already quoted Monte Carlo,[25] especially for low densities, $r_s \geqslant 3a_0$. In any case, the reliability of the surface energies given by these methods is unclear, and which is the *exact* energy of a jellium surface is still an unsolved problem.[27]

So, we can conclude that the mWDA functional, with the proposed ansatz, is the first one that allows us to obtain on the same footing the surface energy, the density profile, and the image behavior of the XC potential of a metallic surface.

ACKNOWLEDGMENTS

The authors acknowledge useful discussions with Dr. J. M. Soler. This work has been partially supported by the Spanish Education Ministry through the DGESIC Grant Nos. PB97-1223-C02-02 and PB97-0077.

APPENDIX: FUNCTIONAL DERIVATIVE OF THE SYMMETRIZED WDA FUNCTIONAL

In general, the functional derivative of $E_{\rm XC}[n]$ can be written as

$$v_{\rm XC}(\mathbf{r}) = V_1(\mathbf{r}) + V_2(\mathbf{r}) + V_3(\mathbf{r}) = \int d\mathbf{r}_1 \frac{n(\mathbf{r}_1)G(\mathbf{r}_1,\mathbf{r})}{2|\mathbf{r}_1-\mathbf{r}|} + \int d\mathbf{r}_1 \frac{n(\mathbf{r}_1)G(\mathbf{r},\mathbf{r}_1)}{2|\mathbf{r}_1-\mathbf{r}|} + \int d\mathbf{r}_1 d\mathbf{r}_2 \frac{n(\mathbf{r}_1)n(\mathbf{r}_2)}{2|\mathbf{r}_1-\mathbf{r}_2|} \frac{\delta G(\mathbf{r}_1,\mathbf{r}_2)}{\delta n(\mathbf{r})}.$$

In the sWDA model, $G(\mathbf{r}_1,\mathbf{r}) = G(\mathbf{r},\mathbf{r}_1)$. Therefore, $V_1(\mathbf{r}) = V_2(\mathbf{r}) = \varepsilon_{\rm XC}(\mathbf{r})$, $\varepsilon_{\rm XC}(\mathbf{r})$ being the XC energy per particle at the point $\mathbf{r}$. On the other hand, according to Eq. (7), $V_3(\mathbf{r})$ is equal to

$$V_3(\mathbf{r}) = \int d\mathbf{r}_1 d\mathbf{r}_2 \frac{G_\xi(\mathbf{r}_1,\mathbf{r}_2)}{2|\mathbf{r}_1-\mathbf{r}_2|} \sum_{n=1}^{2} \xi_n(\mathbf{r}_1,\mathbf{r}_2) \frac{\delta \tilde{k}_F(\mathbf{r}_n)}{\delta n(\mathbf{r})},$$

where $\xi_n(\mathbf{r}_1,\mathbf{r}_2) = \partial\xi(\mathbf{r}_1,\mathbf{r}_2)/\partial \tilde{k}_F(\mathbf{r}_n)$ can be obtained from Eq. (8), and

$$G_\xi(\mathbf{r}_1,\mathbf{r}_2) = n(\mathbf{r}_1)n(\mathbf{r}_2) \frac{\partial G(\mathbf{r}_1,\mathbf{r}_2)}{\partial \xi(\mathbf{r}_1,\mathbf{r}_2)}. \tag{A1}$$

To obtain the matrix $\Xi(\mathbf{r}',\mathbf{r}) = \delta \tilde{k}_F(\mathbf{r}')/\delta n(\mathbf{r})$, we make the functional derivative of the relation (4), arriving at

$$-n(\mathbf{r}_1)G(\mathbf{r}_1,\mathbf{r}) = \int d\mathbf{r}_2 B(\mathbf{r}_1,\mathbf{r}_2)\Xi(\mathbf{r}_2,\mathbf{r}),$$

where the matrix B is given by

$$B(\mathbf{r}_1,\mathbf{r}_2) = G_\xi(\mathbf{r}_1,\mathbf{r}_2)\xi_2(\mathbf{r}_1,\mathbf{r}_2) + \delta(\mathbf{r}_1-\mathbf{r}_2) \times \int d\mathbf{r}_3 G_\xi(\mathbf{r}_1,\mathbf{r}_3)\xi_1(\mathbf{r}_1,\mathbf{r}_3).$$

Therefore, $\Xi(\mathbf{r}_2,\mathbf{r})$ can be found out after a matrix inversion.

The previous set of equations greatly simplifies when considering a jellium surface. In this case, the XC energy per surface unit and the sum rule (7) can be written as

$$e_{\rm XC}[n] = \int dz_1 dz_2 n(z_1)n(z_2)\omega(z_1,z_2) \tag{A2}$$

$$-1 = \int dz_2 n(z_2)\sigma(z_1,z_2), \tag{A3}$$

where

$$\omega(z_1,z_2) = \frac{\pi C(\xi(z_1,z_2))}{2\xi(z_1,z_2)} \int_{2\xi(z_1,z_2)|z_1-z_2|}^{+\infty} dx\, \hat{G}(x),$$

$$\sigma(z_1,z_2) = \frac{\pi C(\xi(z_1,z_2))}{2\xi(z_1,z_2)^2} \int_{2\xi(z_1,z_2)|z_1-z_2|}^{+\infty} dx\, x\hat{G}(x).$$

As a consequence,

$$v_{\mathrm{XC}}(z)=2\int dz_1 n(z_1)\omega(z_1,z)+\int dz_1 dz_2 \omega_{\xi}(z_1,z_2) \times\sum_{n=1}^{2}\xi_n(z_1,z_2)\Xi(z_n,z), \tag{A4}$$

and the matrix Ξ is now the solution of

$$-n(z_1)\sigma(z_1,z)=\int dz_2 b(z_1,z_2)\Xi(z_2,z), \tag{A5}$$

with

$$b(z_1,z_2)=\sigma_{\xi}(z_1,z_2)\xi_2(z_1,z_2)+\delta(z_1-z_2) \times\int dz_2\sigma_{\xi}(z_1,z_2)\xi_1(z_1,z_2).$$

The subindex ξ in σ_{ξ} and ω_{ξ} has the same meaning as that given in Eq. (A1). Note that the integral character of Eq. (A5) avoids a simple analysis of the asymptotic behavior of $v_{\mathrm{XC}}(z)$. In fact, the constant term contained in $v_{\mathrm{XC}}(z\gg 0)$ arises from the nonlocal contribution $V_3(z)$.

[1] P. Hohenberg and W. Kohn, Phys. Rev. **136**, B864 (1964); W. Kohn and L.J. Sham, Phys. Rev. **140**, A1133 (1965).
[2] P.M. Echenique and R.M. Pendry, J. Phys. C **11**, 2065 (1978).
[3] M. Heinrichsmeier, A. Fleszar, W. Hanke, and A.G. Eguiluz, Phys. Rev. B **57**, 14 974 (1998).
[4] N.D. Lang and W. Kohn, Phys. Rev. B **1**, 4555 (1970).
[5] J.P. Perdew, J. Chevary, S.H. Vosko, K.A. Jackson, M.R. Pederson, D.J. Singh, and C. Fiolhais, Phys. Rev. B **46**, 6671 (1992).
[6] P.A. Serena, J.M. Soler, and N. García, Phys. Rev. B **34**, 6767 (1986); **37**, 8701(E) (1988).
[7] L.J. Sham and M. Schlüter, Phys. Rev. Lett. **51**, 1888 (1983); Phys. Rev. B **32**, 3883 (1985).
[8] L. Hedin, Phys. Rev. **139**, A796 (1965).
[9] A.G. Eguiluz and W. Hanke, Phys. Rev. B **39**, 10 433 (1989).
[10] A.G. Eguiluz, M. Heinrichsmeier, A. Fleszar, and W. Hanke, Phys. Rev. Lett. **68**, 1359 (1992).
[11] A. Solomatin and V. Sahni, Phys. Lett. A **212**, 263 (1996).
[12] J.D. Talman and W.F. Shadwick, Phys. Rev. A **14**, 36 (1976).
[13] I.D. White, R.W. Godby, M.M. Rieger, and R.J. Needs, Phys. Rev. Lett. **80**, 4265 (1998).
[14] U. von Barth and B. Holm, Phys. Rev. B **54**, 8411 (1996).
[15] A. Schindlmayr, Phys. Rev. B **56**, 3528 (1997).
[16] O. Gunnarsson, M. Jonson, and B.I. Lundqvist, Phys. Rev. B **20**, 3136 (1979).
[17] J. A. Alonso and N. A. Cordero, in *Recent Developments and Applications of Modern Density Functional Theory*, edited by J. M. Seminario (Elsevier, Amsterdam, 1996).
[18] E. Chacón and P. Tarazona, Phys. Rev. B **37**, 4013 (1988).
[19] J.P. Perdew and Y. Wang, Phys. Rev. B **46**, 12 947 (1993).
[20] O. Gunnarsson and R.O. Jones, Phys. Scr. **21**, 394 (1980).
[21] S. Ossicini, C.M. Bertoni, and P. Gies, Europhys. Lett. **1**, 661 (1986); S. Ossicini, F. Finicchi, and C.M. Bertoni, Surf. Sci. **189/190**, 776 (1987).
[22] P. Tarazona and E. Chacón, Nuovo Cimento D **9**, 589 (1987).
[23] E. Chacón and P. Tarazona, Phys. Rev. B **37**, 4020 (1988).
[24] P. García-González, J.E. Alvarellos, and E. Chacón, Phys. Rev. A **54**, 1897 (1996); Phys. Rev. B **57**, 4857 (1998); Phys. Rev. A **57**, 4192 (1998).
[25] P.H. Acioli and D.M. Ceperley, Phys. Rev. B **54**, 17 199 (1996).
[26] E. Krostscheck and W. Kohn, Phys. Rev. Lett. **57**, 862 (1986); E. Krostscheck, W. Kohn, and G.X. Qia, Phys. Rev. B **32**, 5693 (1985).
[27] Z. Yan, J.P. Perdew, S. Kurth, C. Fiolhais, and L. Almeida, Phys. Rev. B **61**, 2595 (2000).